PROCEEDINGS OF SCIENCE

MUSIC: a detector concept for 10 TeV $\mu^+\mu^-$ collisions

P. Andreetto,[a] **M. Casarsa,**[b,*] **A. Gianelle,**[a] **D. Lucchesi,**[a,c] **L. Palombini,**[a,c] **L. Sestini**[d] **and D. Zuliani**[a,c]

on behalf of the International Muon Collider Collaboration

[a] *INFN - Sezione di Padova, via F. Marzolo 8, 35131 Padua, Italy*
[b] *INFN - Sezione di Trieste, via A. Valerio 2, 34127 Trieste, Italy*
[b] *Università di Padova, via F. Marzolo 8, 35131 Padua, Italy*
[d] *INFN - Sezione di Firenze, via B. Rossi 3, 50019 Sesto Fiorentino, Florence, Italy*

E-mail: massimo.casarsa@ts.infn.it

The full exploitation of the physics potential of a multi-TeV muon collider will ultimately depend on the detector's ability to cope with unprecedented levels of machine-induced backgrounds. This contribution introduces the MUSIC (MUon System for Interesting Collisions) detector concept and presents its performance in the context of $\sqrt{s}$ = 10 TeV muon–antimuon collisions. The MUSIC detector is designed to mitigate machine-induced background effects while maintaining high efficiency and accuracy in the reconstruction of physics events, particularly in the Higgs boson sector and in searches for new physics. It features an all-silicon tracking system, a semi-homogeneous lead-fluorite crystal electromagnetic calorimeter, an iron–scintillator sampling hadronic calorimeter, and a superconducting magnet providing a 5 T magnetic field. Detailed detector simulations including the dominant machine-induced backgrounds are presented. The results demonstrate promising tracking efficiency, as well as muon, photon, electron, and jet reconstruction capabilities, together with jet flavor identification performance, highlighting the strong potential of the detector for high-energy muon collider experiments.

The European Physical Society Conference on High Energy Physics (EPS-HEP2025)
7-11 July 2025
Marseille, France

*Speaker

PoS(EPS-HEP2025)515

1. Introduction

A muon collider represents the most appealing option for achieving leptonic collisions at multi-TeV center-of-mass energies with a relatively compact circular machine [1]. Such high-energy $\mu^+\mu^-$ collisions would unlock an exceptional physics program, enabling high-precision tests of the Standard Model in an unexplored energy regime, probing the structure of the Higgs sector and the shape of the Higgs potential, and allowing both direct and indirect searches for new physics. However, the inherently unstable nature of muons introduces unique background conditions. Fully realizing the physics potential of a multi-TeV muon collider will depend critically on the detector's capability to handle unprecedented levels of machine-induced backgrounds.

The detector requirements driven by physics considerations are broadly aligned with those of other future multi-TeV colliders. These include the ability to reconstruct boosted physics objects originating from Standard Model processes, as well as central, high-energy objects produced in the decays of potential new massive states. In addition, the detector must be capable of identifying unconventional experimental signatures such as disappearing tracks, displaced leptons, displaced photons, and jets. On the machine side, constraints arise from the design of the interaction region and the machine-detector interface, notably the placement of final focusing quadrupoles at ± 6 m from the interaction point. Furthermore, the unique background conditions induced by the muon beams necessitate dedicated mitigation strategies to ensure robust detector performance and preserve sensitivity to the full breadth of the physics program. Ultimately, the detector design, the technological choices, and the development of the event reconstruction algorithms will be driven by the high levels of machine-induced background [2].

The two dominant sources of machine-induced backgrounds are the decay of muons circulating in the machine and the incoherent production of e^+e^- pairs from the interactions of real or virtual photons emitted by the two colliding beams. Further details are provided in Ref. [3].

2. The MUSIC detector concept

The MUSIC (MUon System for Interesting Collisions) detector is designed and optimized for $\mu^+\mu^-$ collisions at a center-of-mass energy of 10 TeV. Its geometry follows the typical cylindrical layout of multipurpose collider experiments, with a length of 11.4 m and a diameter of 12.8 m. From the innermost region outward, it consists of an all-silicon tracking system, an electromagnetic and hadronic calorimeter, and an outer muon system. A superconducting solenoid, located between the electromagnetic and hadronic calorimeters, provides a 5 T magnetic field chosen to mitigate the impact of incoherent e^+e^- pair production on the tracking system. Along the beamline inside the detector volume, two conical tungsten shields, referred to as "nozzles", are placed on either side of the interaction point to protect the detector from the high-energy products of muon decays. A right-handed coordinate system is adopted, with the origin at the detector center (the nominal collision point): the z-axis follows the direction of the clockwise-circulating μ^+ beam, the y-axis points upward, and the x-axis lies in the plane of the collider ring.

The MUSIC detector is illustrated in Fig. 1. Starting from the innermost region, it comprises:

Vertex Detector: It is the innermost system, consisting of five central cylindrical layers, each 26 cm long, positioned at radii ranging from 2.9 to 10.1 cm from the beam axis. The forward and

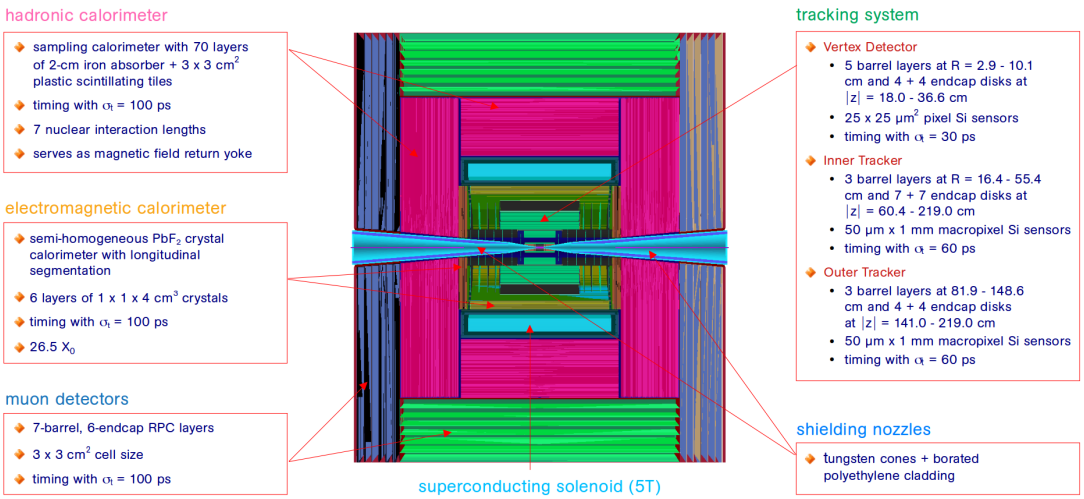

Figure 1: The MUSIC detector.

backward regions feature four disks, oriented transverse to the beamline and located at distances of $|z| = 18.0$ to 36.6 cm from the interaction point. A layout of 25×25 μm^2 pixels is assumed with a hit spatial resolution of 5 μm × 5 μm and a hit time resolution of 30 ps.

Inner Tracker: It consists of 50 μm × 1 mm macropixel modules arranged in three barrel layers, at radii from 16.4 to 55.4 cm, and seven disks on either side at $|z|$ from 60.4 to 219.0 cm. The first two barrel layers are 96.32 cm long, while the third measures 138.46 cm. Hit spatial and time resolutions of 7 μm × 90 μm and 60 ps are assumed, respectively.

Outer Tracker: It has three 252.8-cm long barrel layers at radii between 81.9 and 148.6 cm and four endcap disks at $|z|$ from 141.0 to 219.0 cm. It features 50 μm × 1 mm macropixel with a hit spatial resolution of 7 μm × 90 μm and a hit time resolution of 60 ps.

Electromagnetic calorimeter (ECAL): The ECAL is a semi-homogeneous electromagnetic crystal calorimeter with longitudinal segmentation (CRILIN [4]). It consists of $1 \times 1 \times 4$-cm^3 lead-fluorite crystals arranged in six layers for a total of 26.5 radiation lengths. The cylindrical barrel section has an inner radius of 169.0 cm and is 442.0 cm long. The endcaps, shaped as disks, have inner and outer radii of 31.0 cm and 196.0 cm, respectively, and are positioned at $|z| = 230.7$ cm. The hit time resolution is assumed to be 100 ps.

Hadronic calorimeter (HCAL): It is an iron-scintillator sampling calorimeter composed of 70 layers of 2-cm iron absorbers and 3×3 cm^2 scintillator pads, each 0.3 cm thick, totaling approximately 7 nuclear interaction lengths. It consists of a central cylindrical part measuring 501.8 cm in length and 290.2 cm in radius, along with two endcaps positioned at $|z| = 257.9$ cm. The endcaps have inner and outer radii of 32.0 cm and 475.6 cm, respectively. A hit time resolution of 100 ps is assumed. The HCAL iron absorber also serves as the return yoke for the magnetic field.

Muon system: The current detector is modeled on the resistive-plate chambers (RPCs) employed in the CLIC detector [5]. It features seven barrel layers, each measuring 888.8 cm in length, with radii ranging from 480.6 cm to 680.0 cm, and six endcap layers at $|z|$ positions between 444.4 cm and 590.0 cm, with inner and outer radii of 49.3 cm and 680.0 cm, respectively. The RPCs are segmented into 3×3 cm^2 cells, with a hit time resolution assumed to be 100 ps.

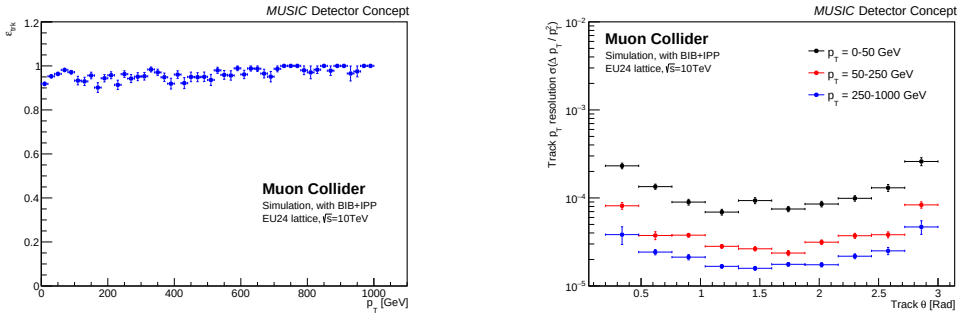

Figure 2: Left: Track reconstruction efficiency for muons as a function of the muon transverse momentum. Right: Transverse momentum resolution as a function of the muon polar angle in three ranges of p_T. To suppress fake tracks from machine-induced backgrounds, cuts of $p_T > 1$ GeV and $|d_0| < 0.1$ mm are applied.

3. MUSIC detector performance

The performance of the MUSIC detector has been assessed through detailed simulations based on GEANT4 [6], including backgrounds from muon decays (beam-induced background, BIB) and incoherent e^+e^- pair production (IPP). BIB is generated with the FLUKA toolkit [7], which models the machine lattice and machine-detector interface of a 10 TeV collider in the "EU24 lattice" configuration [3]. IPP is produced with the Guinea-Pig generator [8], while the propagation and interactions of the resulting electrons and positrons with the nozzles are simulated using FLUKA.

As the closest subdetector to the beamline, the tracking system is most affected by machine-induced backgrounds, especially in the innermost vertex-detector layer, where about 5000 spurious hits/cm^2 are expected within a $[-0.5, 15]$ ns readout window. To mitigate this, tighter timing cuts select hits consistent with particles from the interaction point, within $[-3\sigma_t, +5\sigma_t]$, where σ_t is the hit time resolution. Tracks are reconstructed with a Combinatorial Kalman Filter in the ACTS package [9]. Tracking performance has been studied using samples of single muons, with BIB and IPP overlaid on an event-by-event basis. As shown in the left panel of Fig. 2, the tracking reconstruction efficiency exceeds 95% over a broad range of muon transverse momenta $p_T = p \sin\theta$. The resolution $\Delta p_T/p_T^2$, illustrated in the right panel of Fig. 2, reaches a few 10^{-5} for $p_T > 50$ GeV in the central region of the tracking system, and gradually deteriorates at lower momenta and at polar angles closer to the beamline. Muons are identified by matching tracks to hits in the outer muon system, reaching an identification efficiency above 90% for $p_T > 5$ GeV.

The ECAL is subject to a diffuse, nearly uniform machine-induced background, primarily composed of soft photons. In the first barrel layer, the average energy density is about 400 MeV/cm^2, while the endcaps receive roughly an order of magnitude less. To reduce its impact, hit thresholds based on arrival time and energy are optimized across ECAL layers and polar-angle regions. ECAL hits are clustered using the PandoraPFA package's particle-flow algorithm [10], followed by cluster energy corrections based on energy and polar angle to address reconstruction inefficiencies and detector-related effects. Photon candidates are defined as ECAL clusters without corresponding tracks, consistent with the expectation for neutral particles, while electrons are identified as electromagnetic clusters matched to reconstructed tracks. The photon reconstruction efficiency versus energy is shown in Fig. 3 (left). The estimated relative energy resolution, displayed in the right

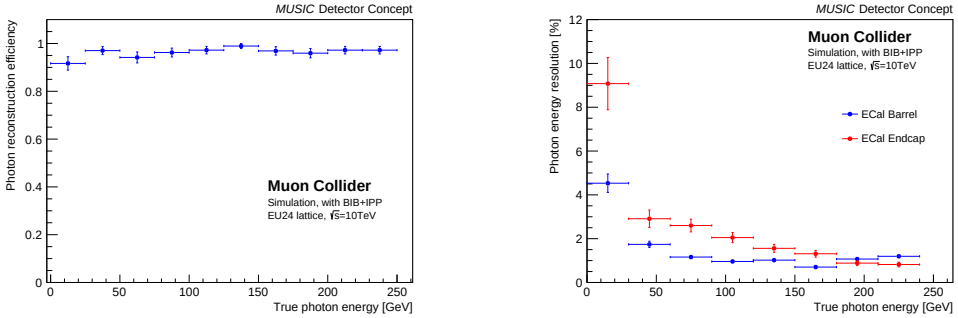

Figure 3: Left: Photon reconstruction efficiency as a function of photon energy in a sample of single photons. Right: Photon energy resolution in ECAL barrel and endcaps as a function of photon energy.

panel, is $10\%/\sqrt{E\,[\mathrm{GeV}]}$ in the barrel and $17\%/\sqrt{E\,[\mathrm{GeV}]}$ in the endcaps, affected by higher background levels. Electron identification efficiency, largely determined by the tracking efficiency, is about 85% for $E > 20\,\mathrm{GeV}$. The energy resolution is consistent with that obtained for photons.

Hadronic jets are complex experimental objects whose reconstruction relies on information from all subdetectors. Jet reconstruction begins with tracks and ECAL/HCAL clusters that, after applying minimal cleaning criteria, serve as inputs to the PandoraPFA particle-flow algorithm. The resulting particle-flow objects are then clustered into jets using the k_t algorithm [11] with $R = 0.5$. The jet four-momentum is obtained by summing the four-momenta of its constituents. To account for detector effects and reconstruction biases, jets are calibrated by applying corrections to the jet p_T and, in the barrel–endcap transition region, to the jet direction. Jets originating from b quarks are tagged using deep neural networks that exploit characteristic signatures of b-hadron decays, such as displaced secondary vertices within the jet and the presence of displaced muons. Jet reconstruction and b-tagging performance have been evaluated using samples of $b\bar{b}$, $c\bar{c}$, and light-quark dijet events, generated with Pythia [12] and fully simulated and reconstructed, including BIB and IPP. Jet reconstruction efficiency as a function of jet polar angle is shown in the top left panel of Fig. 4 for different jet flavors, reaching nearly 100% in the central region. The p_T resolution for central jets, shown in Fig. 4 (top right), is about 30% at $p_T \sim 20\,\mathrm{GeV}$ and improves to 10% at $p_T \sim 200\,\mathrm{GeV}$. At low p_T, the resolution degrades to approximately 45% in the barrel-endcap transition regions and in the endcaps. Figure 4 (bottom left) shows the b-tagging efficiency as a function of the true quark p_T for jets originating from b-, c-, and light-flavor quarks. At a representative working point, the average efficiency is 55% for b-jets, 20% for c-jets, and 0.8% for light-flavor jets.

Detector performance was further assessed through full-fledged physics analyses in the Higgs sector [13]. As an example, Fig. 4 (bottom right) shows the current separation between the reconstructed dijet invariant-mass peaks for the Z and H bosons.

Acknowledgments

This work was supported by the European Union's Horizon 2020 and Horizon Europe Research and Innovation programs through the Marie Skłodowska-Curie RISE Grant Agreement No. 101006726 and the Research Infrastructures INFRADEV Grant Agreement No. 101094300.

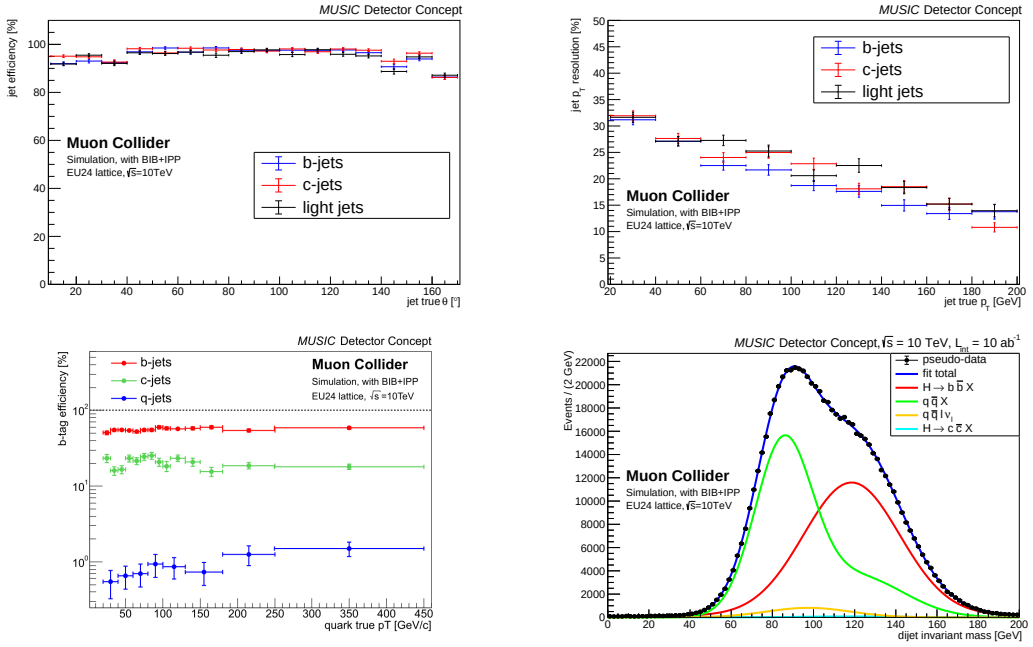

Figure 4: Top: Reconstruction efficiency as a function of the generator-level jet polar angle (left) and energy resolution as a function of generator-level jet p_T in the central region $60^\circ < \theta_{\text{jet}} < 120^\circ$ (right) for b, c, and light-flavor jets. Bottom left: Efficiency of the b-flavor identification algorithm as a function of the true quark p_T. Bottom right: Reconstructed dijet invariant mass for signal and physics backgrounds in the $H \to b\bar{b}$ channel. BIB and IPP are superimposed on the physics processes on an event-by-event basis.

References

[1] C. Accettura *et al.*, Eur. Phys. J. C 83, 864 (2023).

[2] M. Casarsa, D. Lucchesi, L. Sestini, Annu. Rev. Nucl. Part. Sci. 74, 233 (2024).

[3] D. Calzolari *et al.*, PoS ICHEP2024, 819 (2025).

[4] S. Ceravolo *et al.*, 2022 JINST 17 P09033.

[5] D. Arominski *et al.*, arXiv:1812.07337 (2018).

[6] S. Agostinelli *et al.*, Nucl. Instrum. Meth. A 506, 250 (2003).

[7] C. Ahdida *et al.*, Front. Phys. 9, 788253 (2022).

[8] C. Rimbault *et al.*, EUROTEV-REPORT-2005-016 (2005).

[9] X. Ai *et al.*, Comput. Softw. Big Sci. 6, 8 (2022).

[10] M. Thomson, Nucl. Instrum. Meth. A 611, 25 (2009).

[11] S.D. Ellis and D.E. Soper, Phys. Rev. D 48, 316 (1993).

[12] T. Sjöstrand *et al.*, Comput. Phys. Commun. 191, 159 (2015).

[13] P. Andreetto *et al.*, PoS EPS-HEP2025, 385 (2026).